

Self-supervised Implicit Glyph Attention for Text Recognition

Tongkun Guan¹, Chaochen Gu¹, Jingzheng Tu¹, Xue Yang², Qi Feng¹, Yudi Zhao¹, Wei Shen²

¹ Department of Automation, Shanghai Jiao Tong University

² MoE Key Lab of Artificial Intelligence, AI Institute, Shanghai Jiao Tong University
 {gtk0615,jacygu,tujingzheng,yangxue-2019-sjtu,fengqi,yudizhao,wei.shen}@sjtu.edu.cn

Abstract

The attention mechanism has become the *de facto* module in scene text recognition (STR) methods, due to its capability of extracting character-level representations. These methods can be summarized into implicit attention based and supervised attention based, depended on how the attention is computed, *i.e.*, implicit attention and supervised attention are learned from sequence-level text annotations and character-level bounding box annotations, respectively. Implicit attention, as it may extract coarse or even incorrect spatial regions as character attention, is prone to suffering from an alignment-drifted issue. Supervised attention can alleviate the above issue, but it is category-specific, which requires extra laborious character-level bounding box annotations and would be memory-intensive when the number of character categories is large. To address the aforementioned issues, we propose a novel attention mechanism for STR, self-supervised implicit glyph attention (SIGA). SIGA delineates the glyph structures of text images by jointly self-supervised text segmentation and implicit attention alignment, which serve as the supervision to improve attention correctness without extra character-level annotations. Experimental results demonstrate that SIGA performs consistently and significantly better than previous attention-based STR methods, in terms of both attention correctness and final recognition performance on publicly available context benchmarks and our contributed contextless benchmarks. Code and datasets will be released soon.

Introduction

Scene text recognition (STR) aims to recognize texts from natural images, which has wide applications in handwriting recognition (Wang et al. 2009; Bhunia et al. 2021), industrial print recognition (Guan et al. 2022), and visual understanding (Biten et al. 2019). Recently, attention-based models with encoder-decoder architectures are typically developed to address this task by attending to important regions of text images to extract character-level representations. These methods can be summarized into implicit attention methods (a) and supervised attention methods (b) in Figure 1, according to the annotation type used for supervising the attention.

Specifically, implicit attention is learned from sequence-level text annotations by computing attention scores across all locations over a 1D or 2D space. For example, (Shi et al. 2018; Baek et al. 2019) generated 1D sequential at-

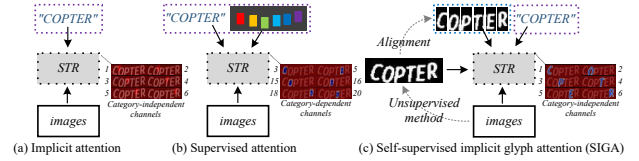


Figure 1: Three different supervised manners for STR.

tention weights at different decoding steps to extract important items of encoded sequence. (Yu et al. 2020; Fang et al. 2021) generated 2D attention weights by executing a cross-attention operation with the embedded time-dependent sequences and visual features on all spatial locations. In addition, supervised attention (Liao et al. 2019; He et al. 2022) is learned from extra character-level bounding box annotations by generating character segmentation maps.

However, implicit attention methods, which only extract coarse or even unaligned spatial regions as character attention, may encounter alignment-drifted attention. Besides, although supervised attention methods can alleviate the above issue, they rely on labour-intensive character-level bounding box annotations, and their category-dependent attention maps might be memory-intensive when the number of character categories is large.

To address the aforementioned issues, we propose a novel attention-based method for STR (Figure 1 (c)), self-supervised implicit glyph attention (SIGA). As briefly shown in Figure 2, SIGA delineates the glyph structures of text images by jointly self-supervised text segmentation and implicit attention alignment, which serve as the supervision for learning attention maps during training to improve attention correctness. Specifically, the glyph structures are generated by modulating the learned text foreground representations with sequence-aligned attention vectors. The text foreground representations are distilled from self-supervised segmentation results according to the internal structures of images (Hartigan and Wong 1979); The sequence-aligned attention vectors are obtained by applying an orthogonal constraint to the 1D implicit attention vectors (Baek et al. 2019). They then serve as the position information of each character in a text image to modulate the text foreground representations to generate glyph pseudo-labels online.

By introducing glyph pseudo-labels as the supervision of

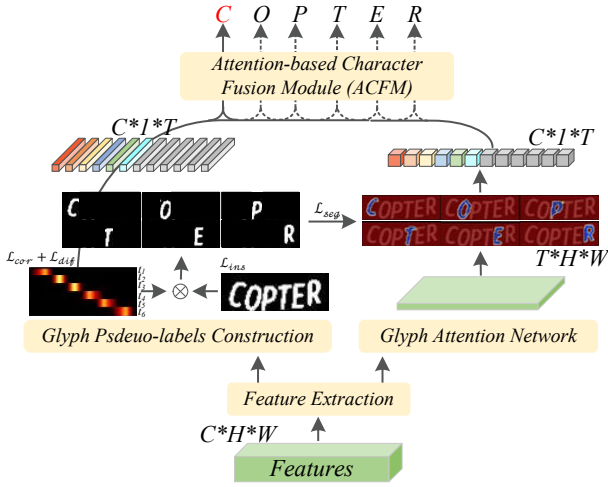


Figure 2: We propose a self-supervised implicit glyph attention method by adding supervision of the online constructed structures of glyphs to the attention module.

attention maps, the learned glyph attention encourages the text recognition network to focus on the structural regions of glyphs to improve attention correctness. Different from supervised attention methods, the glyph attention maps with fixed-length channels have character and order consistency, since the order is ensured and characters are well aligned, which brings no additional cost when handling larger character categories of language.

Benefiting from the glyph attention, our method achieves state-of-the-art results on seven publicly available context benchmarks. We also encapsulate our method as a plug-in component to other attention-based STR methods, achieving performance gains of 5.45% and 1.11% on SRN (Yu et al. 2020) and ABINet (Fang et al. 2021), respectively. To further verify the effectiveness of our method for vision-only text recognition tasks, we contribute two large-scale contextless benchmarks (MPSC and ArbitText) with special spelling rules that differ from legal words. Experiments demonstrate that our method achieves the best performance on these contextless benchmarks. In summary, the main contributions of this paper are as follows:

- We propose a novel attention mechanism for scene text recognition, which is able to delineate glyph structures of text images to improve attention correctness without character-level bounding box annotations.
- Extensive experiments demonstrate that the proposed glyph attention is essential for improving the performance of vision models. Our method achieves competitive performance on publicly available context benchmarks and our contributed large-scale contextless benchmarks (MPSC and ArbitText).

Related Work

Recently, some top-down approaches have been developed to recognize entire images instead of directly recognizing character segments like traditional bottom-up approaches

(Wang and Belongie 2010; Neumann and Matas 2012). These methods can be roughly divided into vision-based and language-based methods.

Vision-based methods: These methods view STR as a character-level classification task and mainly exploit the visual information to recognize texts. (Cheng et al. 2017; Bai et al. 2018; Liu et al. 2018; Shi et al. 2018) execute sequence attention modeling over a 1D space. Specifically, input text images are first encoded into 1D sequential features. Then, they employ a bidirectional decoder to extract attentive features of the encoded sequence by outputting the corresponding attention weights for prediction. Besides, (Li et al. 2019; Lee et al. 2020; Wang et al. 2020; Yu et al. 2020; Fang et al. 2021) develop various 2D attention mechanisms by attending to spatial vision features of each character of an image. Specifically, (Li et al. 2019) combine feature maps and hidden states of the decoder to focus on spatial character features at each decoding step. (Yu et al. 2020; Fang et al. 2021) adopt a transformer-based structure to compute attention scores for all spatial locations of visual features, thereby obtaining attention maps for corresponding characters. However, supervised by sequence-level text annotations, these implicit attention methods easily extract coarse or even unaligned spatial regions as character attention.

In contrast, under the supervision of extra character-level bounding box annotations, (Lyu et al. 2018) and (Wan et al. 2020) employ a fully convolutional network to predict character-level segmentation results and then perform classification tasks. (He et al. 2022) utilizes the segmentation probability maps to exploit spatial context for text reasoning by graph convolutional networks. However, character-level annotations of text images are expensive and laborious. Beyond the limitations of human annotations, we delineate the glyph structures of text images as the supervision of attention maps by jointly self-supervised text segmentation and implicit attention alignment.

Language-based methods: Inspired by natural language processing methods, the visual outputs are fed into a language model by developing a transformer framework to implement recognition correction with linguistic context. (Yu et al. 2020; Bhunia and et al. 2021) stack multiple layers of self-attention structures for semantic reasoning tasks. Inspired by the masked language model (MLM) in BERT (Kenton and Toutanova 2019), (Fang et al. 2021) pre-train the proposed BCN to predict the masked character in text based on linguistic context, and fine-tune visual outputs to improve performance. Although they leverage a language model to optimize the joint character prediction probability with visual models, which reduces prediction errors with linguistic context, they do not generalize well to arbitrary texts (e.g., contextless texts with a specific workpiece coding scheme). Therefore extracting the distinctive visual features of characters is still the key to text recognition.

Methodology

In this section, we first review the representative attention based method that learns the 1D attention weights implicitly (Baek et al. 2019), and then introduce our self-supervised implicit glyph attention method.

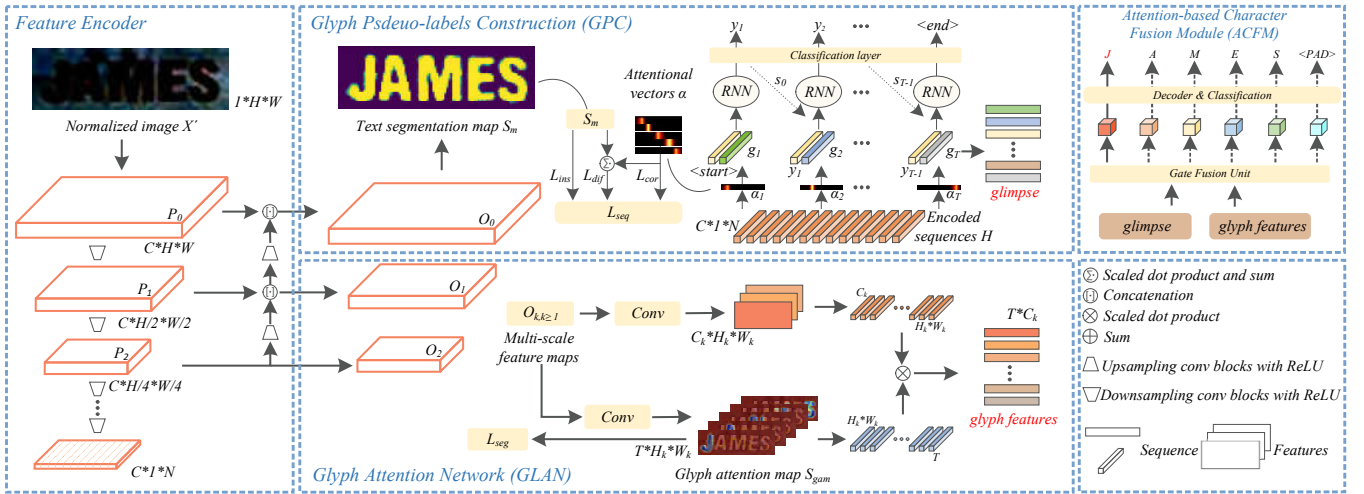


Figure 3: Overview of the proposed self-supervised implicit glyph attention network for text recognition.

Implicit Attention Method over 1D Space

The implicit attention method (Baek et al. 2019) consists of a transformation layer, an encoder and a decoder. First, the transformation layer employs a Thin Plate Spline (TPS), a variant of the spatial transformation network (STN) (Jaderberg et al. 2015), to transform an input image \mathbf{X} into a normalized image \mathbf{X}' . Then, the encoder extracts text features $\mathbf{H} \in \mathbb{R}^{C \times 1 \times N}$ from the normalized image $\mathbf{X}' \in \mathbb{R}^{C \times H \times W}$ by a variant of ResNet (He et al. 2016), and splits the text features into a fixed-length sequence $(\mathbf{h}_i, i = \{1, \dots, N\})$. In the decoder, as illustrated in Figure 4 (a), the encoded sequence is fed into a recurrent module (e.g., LSTM, GRU) to generate an output vector \mathbf{x}_t and a new state vector \mathbf{s}_t at the decoding step t . The specific details are as follows:

$$(\mathbf{x}_t, \mathbf{s}_t) = \text{rnn}(\mathbf{s}_{t-1}, (\mathbf{g}_t, E(y_{t-1}))), \quad (1)$$

where $(\mathbf{g}_t, E(y_{t-1}))$ denotes the combination of *glimpse* \mathbf{g}_t and the embedding vector of the predicted class at the previous decoding step. Especially, y_0 denotes an artificially defined “<start>” token. The *glimpse* is computed by the attention mechanism as follows:

$$\begin{cases} e_{t,i} = \mathbf{w}^\top \tanh(\mathbf{W}\mathbf{s}_{t-1} + \mathbf{V}\mathbf{h}_i + b), \\ \alpha_{t,i} = \exp(e_{t,i}) / \sum_{i'=1}^N \exp(e_{t,i'}), \\ \mathbf{g}_t = \sum_i \alpha_{t,i} \mathbf{h}_i, i = 1, \dots, N, \end{cases} \quad (2)$$

where the $\mathbf{w}, \mathbf{W}, \mathbf{V}$ are learnable parameters. Finally, the output vector \mathbf{x}_t predicts the character classification by a linear layer at the current decoding step t . The decoder is executed T times (i.e., total decoding steps) and outputs classification results sequentially.

Our Self-supervised Implicit Attention Method

In this work, we follow the implicit attention method (Baek et al. 2019) as the baseline structure, and delineate glyph structures of text images as the supervision of our attention network by proposing a novel online glyph pseudo-label

construction module. The learned glyph attention encourages the text recognition network to focus on the structural regions of glyphs to improve attention correctness.

Glyph Pseudo-label Construction (GPC)

For a normalized image, given the text mask of an image and its horizontal position information for each character, we can easily obtain the glyph structures of these characters by computing the dot product between them, instead of labour-intensive pixel-level annotations. Towards the goal, we construct glyph pseudo-labels online by jointly self-supervised text segmentation and implicit attention alignment. Then the sequence-aligned attentions serve as the position information of each character in a text image to modulate the learned text foreground representations to generate them.

1) *Self-supervised Text Segmentation*. In the subsection, we want to learn text foreground representations with morphological structures of glyphs, by a semantic segmentation network that assigns every pixel a foreground or background label on the unlabeled text images. In particular, the underlying morphological representation of glyphs is not affected by slightly structural changes (e.g., thicker or thinner), which reduces the reliance on pixel-level high-precision segmentation with expensive computation and annotation costs. Thus we begin with a clustering task based on the internal structures of text images for obtaining pseudo-labels about text masks. Surprisingly, the morphological structures of glyphs are clustered well in most text images.

Then, the text foreground representations are distilled from self-supervised segmentation results produced by our designed text segmentation network. Specifically, we define the output of *Conv 0*, *Block 0*, and *Block 1* from ResNet as \mathbf{P}_0 , \mathbf{P}_1 , and \mathbf{P}_2 , and a top-down pyramid architecture is employed as follows:

$$\begin{cases} \mathbf{O}_2 = \varphi(\mathbf{P}_2), \\ \mathbf{O}_1 = \varphi([\mathcal{T}(\mathbf{O}_2, s_1), \mathbf{P}_1]), \\ \mathbf{O}_0 = \varphi([\mathcal{T}(\mathbf{O}_1, s_0), \mathbf{P}_0]), \end{cases} \quad (3)$$

where $\varphi(\cdot)$ denotes two convolutional layers with Batch-

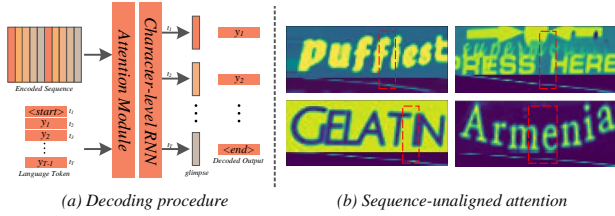


Figure 4: Illustration of the representative attention-based decoder and some sequence-unaligned attention examples. The red dashed boxes in (b) indicate that the attention weight struggles to align text sequence at the current decoding step.

Norm and ReLU activation function, $\mathcal{T}(\cdot)$ refers to single $2\times$ upsampling for \mathbf{O}_k with resolution s_k (i.e., $H_k \times W_k$), and $[\cdot]$ represents the concatenation operation along the channel axis. \mathbf{O}_0 is exploited to produce the text segmentation mask \mathbf{S}_m by a binary classification convolutional layer.

Finally, we employ a binary cross-entropy loss \mathcal{L}_{ins} between \mathbf{S}_m and pseudo-labels about text masks to promote the text segmentation performance. Consequently, the optimized segmentation network perceives the text foreground representations with morphological structures of glyphs in challenging text images, which may be difficult to be classified by an unsupervised clustering method. Some visualization examples are shown in Figure 5. For simplicity, in the experiment, we focus our study on K -means to implement the clustering task, but other clustering approaches with pre-defined categories can be used.

2) *Implicit Attention Alignment.* In the decoding unit (formula 2), the implicit attention weights $\alpha = \{\alpha_t\}_{t=1, \dots, T}$ focus on the important items of the encoded sequence to capture character dependencies. Inspiringly, we transform the attention weights as the position information for the corresponding characters. However, the time information of the decoder is drowned with the other introductions at the latter decoding steps, which easily leads to alignment drift as shown in Figure 4 (b), i.e., the learnable attention weights struggle to align the text sequence (Wang et al. 2020).

To address the issue, we apply an orthogonal constraint to the implicit attention weights to obtain sequence-aligned attention vectors. Specifically, we take these learnable attention weights as vectors and perform an alignment operation by ensuring that they are orthogonal to each other and that every processed vector is aligned with the corresponding character of text segmentation results. Assuming that L denotes the character number of a text image, we first calculate the correlation coefficient S_{cor} between L attention vectors, and then extract the character saliency map \mathbf{S}_{sal} by the attention vectors. The details are as follows:

$$\begin{cases} S_{\text{cor}} = \sum_{1 \leq t < t' \leq L} \alpha_t^T \alpha_{t'}, \\ \beta_t = \xi(\alpha_t), \\ S_{\text{sal}} = \sum_{t=1}^L (\sigma(\beta_t) \cdot \mathbf{S}_m), \end{cases} \quad (4)$$

where ξ represents the one-dimensional linear interpolation ($\xi : \alpha_t \in \mathbb{R}^N \rightarrow \beta_t \in \mathbb{R}^W$). $\sigma(\cdot)$ refers to the nonlinear



Figure 5: Some segmentation examples. (a) denotes the original images, (b) means the results of K -means, and (c) is our text segmentation maps. In the last group of rows, our segmentation module can capture morphological structures of glyphs in challenging images.

activation function, which maps each element in the vector to $[0, 1]$:

$$\sigma(x) = 1 / (1 + \exp(-\mu(x - \lambda))), \quad (5)$$

where μ, λ represent scaling and offset transitions, set to 70 and 0.1 in the experiment, respectively. Then the alignment drift problem can be alleviated by minimizing the correlation coefficient S_{cor} and the difference S_{dif} between \mathbf{S}_m and \mathbf{S}_{sal} by the following loss function:

$$\begin{cases} \mathcal{L}_{\text{cor}} = S_{\text{cor}}, \\ \mathcal{L}_{\text{dif}} = \frac{1}{n} \sum_{i=1}^n -(\rho_i \log(\rho_i^*) + (1 - \rho_i) \log(1 - \rho_i^*)), \\ \mathcal{L}_{\text{seq}} = \mathcal{L}_{\text{cor}} + \mathcal{L}_{\text{dif}}, \end{cases} \quad (6)$$

where n denotes the number of pixels in the text segmentation map \mathbf{S}_m , ρ_i and ρ_i^* are the confidence score of pixel i in \mathbf{S}_m and \mathbf{S}_{sal} , respectively.

Finally, by optimizing the proposed constraint function during training, the attention weights are successfully aligned with the encoded sequence and contribute accurate positional information for glyph pseudo-label construction.

3) *Glyph Pseudo-label Construction.* By calculating the dot product between the aligned attention weights and text segmentation mask \mathbf{S}_m , we obtain the glyph pseudo-labels. Specifically, assuming that the glyph pseudo-label is \mathbf{S}_{gt} , we construct it from the concatenation operation as follows:

$$\mathbf{S}_{\text{gt}} = [1 - \mathbf{S}_m, \mathbb{1}_{[\beta_1 \geq \delta]} \cdot \mathbf{S}_m, \dots, \mathbb{1}_{[\beta_T \geq \delta]} \cdot \mathbf{S}_m], \quad (7)$$

where $[\cdot]$ represents the concatenation operation along the channel axis. δ denotes the confidence threshold, which is set to 0.05 in the experiment. Some visualization examples about the self-constructed \mathbf{S}_{gt} are shown in Figure 6.

Note that the proposed glyph pseudo-label construction module will be removed in the test stage.

Glyph Attention Network (GLAN)

The existing supervised attention methods for STR have the following limitations: 1) For larger character categories of languages, these methods might be memory-intensive and run slower due to their category-dependence character segmentation maps. 2) It is not easy to obtain the character order of text directly from the character segmentation maps predicted by CNNs. An extra order segmentation branch (Wan

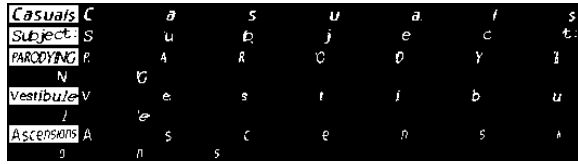


Figure 6: Self-constructed glyph pseudo-labels online.



Figure 7: Comparison of different text benchmarks of STR.

et al. 2020) is introduced to ensure channel and character order consistency, which brings time and computational complexity. 3) Training the segmentation network requires laborious and difficult character-level bounding box annotations.

Benefiting from self-constructed glyph pseudo-labels, our glyph attention network does not have these limitations since the order is ensured and characters are well aligned. The glyph attention network generates glyph attention maps with fixed-length and category-independent channels, whose channel-specific map corresponds to the order-specific glyph attention. Specifically, followed by several convolutional layers, the features O_k in formula 3 are employed to predict glyph attention map S_{gam} with the channel number of N_s . N_s is set to $1 + M$ and not equal to the character categories, which represents the sum of background class and the set maximum character length on text images ($M=26$). For example, to recognize GB2312 with 6763 categories in Chinese, if the same convolution layer is employed and feature channels are 256, the parameter size is 1.7M (256×6763) for supervised attention methods while 6.9K (256×27) for our method.

And then, supervised by the constructed glyph pseudo-labels, we use the joint loss function of multi-class Dice loss (Milletari, Navab, and Ahmadi 2016) and cross-entropy loss to boost the segmentation results of the glyph attention network. The specific details are as follows:

$$\begin{cases} \mathcal{L}_{\text{dice}} = \frac{1}{L} \sum_{j=2}^{L+1} \left(1 - \frac{2 \sum_{i=1}^n (\omega_{j,i} \omega_{j,i}^*)}{\sum_{i=1}^n (\omega_{j,i}) + \sum_{i=1}^n (\omega_{j,i}^*)} \right), \\ \mathcal{L}_{\text{cel}} = \frac{-1}{n} \sum_{i=1}^n (\rho_i \log(\sum_{j=2}^{M+1} \omega_{j,i}^*) + (1 - \rho_i) \log(1 - \sum_{j=2}^{M+1} \omega_{j,i}^*)), \\ \mathcal{L}_{\text{seg}} = \mathcal{L}_{\text{dice}} + \mathcal{L}_{\text{cel}}, \end{cases} \quad (8)$$

where $\omega_{j,i}$ and $\omega_{j,i}^*$ are the confidence scores of pixel i of the j -index map in the pseudo-label S_{gt} and glyph attention map S_{gam} , respectively. ρ_i is the confidence score of pixel i in S_m . L denotes the character numbers of text images.

Finally, the learned glyph attention encourages the recognition branch to focus on the structural regions of glyphs to extract glyph features for STR, which contain more robust and discerning character representations. Specifically, the encoded text features $O_k \in \mathbb{R}^{W_k \times H_k \times C}$ is first fed into

Table 1: The parameter setting table of SIGA.

Name	Value	Name	Value
Decoding step T	26	Sequence length N	32
Feature channel C	256	Max character length M	26
Image size W, H	128, 32	Constant λ, μ	0.1, 70
Confidence threshold δ	0.05	Constant k	2

two convolutional layers with BatchNorm and ReLU activation function, and then multiplied with character segmentation maps $S_{\text{gam}} \in \mathbb{R}^{W_k \times H_k \times M}$ (remove background) to obtain glyph features $I_k \in \mathbb{R}^{M \times C}$.

Attention-based Character Fusion Module (ACFM)

As discussed above, the visually aligned *glimpse* g_t and glyph features $I_{k,t}$ denote two different character feature representations. Considering that their contributions to STR should be different among various text images, inspired by the gate unit (Arevalo et al. 2017), we dynamically fuse the sequence $I_{k,t}$ and *glimpse* g_t to enrich the semantic information for character recognition at the decoding step t . Finally, we embed these final sequences into the decoder (Baek et al. 2019) to output the current decoded classification results.

Experiments

Datasets and Implementation Details

Our model is trained on two large-scale synthetic datasets (*i.e.*, SynthText (Gupta, Vedaldi, and Zisserman 2016), MJSynth (Jaderberg et al. 2014)) to fairly comparison. Nine STR datasets are used to evaluate the performance of our method, including seven publicly available context benchmarks (Baek et al. 2019) (*i.e.*, IIIT5K-Words, ICDAR2003, ICDAR2013, Street View Text, ICDAR2015, SVT Perspective, and CUTE80) and two new contextless benchmarks (MPSC and ArbitText). The differences between context and contextless benchmarks are shown in Figure 7.

MPSC: We cropped 15003 real-world industrial text instances (larger than the sum of seven context benchmark samples) from industrial text images provided by MPSC (Guan et al. 2022). These texts contain special spelling rules with low semantic relationships for marking workpiece information (*e.g.*, “YS6Q-6615-AD”).

ArbitText: We also synthesize a contextless ArbitText with one million images that each sample is generated by random combination with English letters and Arabic numerals.

Our proposed method is implemented on a server with 2 NVIDIA V100 GPUs in PyTorch. Specifically, we adopt the Adam optimizer (Kingma and Ba 2014) and the one-cycle learning rate scheduler (Smith and Topin 2019) with a maximum learning rate of 0.0005 to train our model. The parameter details are shown in Table 1.

Comparisons on context benchmarks

Vision model. We compare with the previous state-of-the-art methods to evaluate the effectiveness of our method on standard context benchmarks. As shown in Table 2, our method achieves state-of-the-art performance on eight

Table 2: Comparison results of STR methods. * denotes an unclear version of the current dataset is evaluated. † represents the visual model performance within the scope of this paper for a fair comparison. The best results are shown in **bold font**.

Methods	Venue	IIIT	SVT	IC03		IC13		IC15		SP	CT
		3000	647	860	867	857	1015	1811	2077	645	288
CRNN (Shi, Bai, and Yao 2016)	TPAMI	78.2	80.8	89.4	-	-	86.7	-	-	-	-
RARE (Shi et al. 2016)	CVPR	81.9	81.9	90.1	-	88.6	-	-	-	71.8	59.2
ASTER (Shi et al. 2018)	TPAMI	93.4	93.6	94.5	-	-	91.8	-	76.1*	78.5	79.5
ScRN (Yang et al. 2019)	ICCV	94.4	88.9	95.0	-	-	93.9	-	78.7	80.8	87.5
MORAN (Luo, Jin, and Sun 2019)	PR	91.2	88.3	-	95.0	-	92.4	-	68.8	-	77.4
SAR (Li et al. 2019)	AAAI	91.5	84.5	-	-	-	91.0	-	69.2	76.4	83.3
CA-FCN(Liao et al. 2019)	AAAI	91.9	86.4	-	-	-	91.5	-	-	-	79.9
DAN (Wang et al. 2020)	AAAI	94.3	89.2	-	95.0	-	93.9	-	74.5	80.0	84.4
TextScanner (Wan et al. 2020)	AAAI	93.9	90.1	-	-	-	92.9	-	79.4*	84.3	83.3
SE-SAR (Qiao et al. 2020)	CVPR	-	85.8	-	-	-	90.9	-	73.4	78.7	-
SRN† (Yu et al. 2020)	CVPR	92.3	88.1	-	-	-	93.2	77.5	-	79.4	84.7
PlugNet (Mou et al. 2020)	ECCV	94.4	92.3	95.7	-	-	95.0	-	82.2	84.3	85.0
ViTSTR (Atienza 2021)	ICDAR	88.4	87.7	94.7	94.3	93.2	92.4	78.5	72.6	81.8	81.3
TRBA (Baek, Matsui, and Aizawa 2021)	CVPR	92.1	88.9	94.8	95.1	93.9	93.1	78.3	74.7	79.5	78.2
GA-SPIN (Zhang et al. 2021)	AAAI	95.2	90.9	94.9	-	-	94.8	82.8	79.5	83.2	87.5
PIMNet (Qiao et al. 2021)	ACM MM	95.2	91.2	-	-	95.2	93.4	83.5	81.0	84.3	84.4
ABINet† (Fang et al. 2021)	CVPR	94.7	91.7	94.3	94.7	95.0	93.6	82.7	83.0	85.1	86.5
S-GTR† (He et al. 2022)	AAAI	94.0	91.2	-	-	94.8	-	82.8	-	85.0	88.4
SIGA (ours)	-	95.7	93.8	96.8	96.0	96.2	94.7	84.3	80.9	86.2	90.0

Table 3: Comparison results of scene text recognition methods using real-world data in the training stage.

Datasets	IIIT	SVT	IC13		IC15		SP	CT
	3000	647	857	1015	1811	2077	645	288
Methods	3000	647	857	1015	1811	2077	645	288
SAR	95.0	91.2	-	94.0	-	78.8	86.4	89.6
TextScanner	95.7	92.7	-	94.9	83.5	-	84.8	91.6
RobustScanner	95.4	89.3	-	94.1	-	79.2	82.9	92.4
SIGA (ours)	96.8	94.0	96.8	96.3	86.3	83.0	87.3	92.8

Table 4: Comparison results of language methods.

Datasets	IIIT	SVT	IC13		IC15		SP	CT
	3000	647	857	1015	1811	2077	645	288
Methods	3000	647	857	1015	1811	2077	645	288
SRN	94.8	91.5	-	95.5	82.7	-	85.1	87.8
Bhumia et al. (2021)	95.2	92.2	-	95.5	-	84.0	85.7	89.7
Wang et al. (2021)	95.8	91.7	-	95.7	83.7	-	86.0	88.5
S-GTR	95.1	93.2	95.9	-	84.1	-	86.2	91.3
ABINet	96.2	93.5	97.4	-	86.0	-	89.3	89.2
SIGA (ours)	96.2	94.9	97.7	96.2	85.8	82.2	88.8	92.4

context benchmark datasets. Specifically, compared to supervised attention methods (CA-FCN, TextScanner), our method doesn't need extra character-level annotations and brings significant performance gains (1.5% ~ 10.1%) on these benchmarks. Compared to implicit attention methods, our method has better performances and outperforms the best results of previous methods on IIIT, IC03-860, IC03-867, IC13-857, IC15-1811, SP and CT benchmarks by 0.5%, 1.1%, 0.9%, 1.0%, 0.8%, 1.1%, 1.6%, respectively. These results demonstrate that our method extracts more discerning visual features by introducing glyph attention.

We also add the training set of real-world datasets to train our method. As shown in Table 3, our method achieves the best performance compared to the reported results of other STR methods trained on real-world datasets, which demonstrates the feasibility and effectiveness of our method training on real data.

Language model. The semantic reasoning task of language models corrects visual outputs to reduce prediction errors with linguistic context, which improves the overall recogni-

Table 5: Comparison results of contextless benchmarks.

Methods	SAR	DAN	GA-SPIN	PIMNet	ABINet†	SIGA (ours)
Datasets	SAR	DAN	GA-SPIN	PIMNet	ABINet†	SIGA (ours)
MPSC (15003)	59.7	57.7	51.7	60.8	64.4	65.6
ArbitText (1M)	64.5	61.0	54.0	61.1	61.8	66.0

tion accuracy on context benchmarks. In the experiment, we deploy the transformer-based language model of ABINet for language modelling on our vision model. Compared to other visual-language methods, our method achieves competitive results in Table 4 despite not using the official pretrained language model file provided by ABINet.

Comparisons on contextless benchmarks

To verify the effectiveness of our method on the vision-only text recognition tasks, we conduct experiments on our contributed large-scale contextless benchmarks, which will be released publicly to facilitate generalization research on contextless text. These texts have low semantic relationships that are different from the legal spelling of words, which still have a wide range of application scenarios, such as work-piece marking information and identification codes. Thus language-based methods that build implicit language representations with linguistic context are unsuitable for these contextless texts. Exploiting the visual features of text images is essential for improving recognition accuracy.

As shown in Table 5, our method achieves the best performance on the real-world MPSC benchmark compared to other vision-based methods. In particular, we also synthesize a large-scale contextless benchmark, ArbiText, to evaluate the generality and effectiveness of vision models on vision-only tasks. As a result, SIGA shows its prominent superiority and achieves performance improvement of 4.9% and 4.2% compared to PIMNet and ABINet†, respectively. These results consistently emphasize that the proposed glyph attention is essential for improving the performance of visual models.

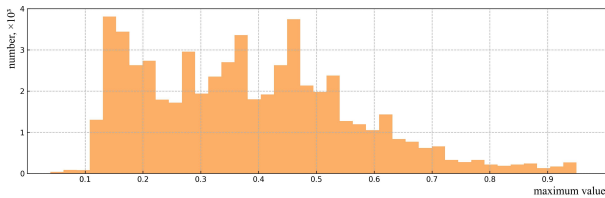


Figure 8: The distribution result of maximum value of α .



Figure 9: Extensive 2D attention visualization results generated by ABINet (a) and SIGA (b).

Ablation Study

Hyper-parameters. The hyper-parameters map the attention weights α to different numerical ranges. For λ and μ of Eq. 5, they encode α to $[0, 1]$ for generating S_{sal} (Minimizing the difference between S_{sal} and S_m to alleviate the alignment drift problem). For δ of Eq. 7, it binarizes α to 0 or 1 for constructing S_{gt} (Obtaining the glyph pseudo-labels). To further observe the attention weight values α , we also statistically analyze the distribution of the maximum value of α on the validation set, as shown in Figure 8. Thus the hyper-parameters are easily set to reasonable values based on the prior distribution. Specifically, we set the confidence threshold δ to 0.05, 0.1, and 0.15, respectively, and the average accuracy on seven context benchmarks is 90.75%, 90.29% and 89.75%. For μ and λ of Eq. 5, we set the three suitable parameter pair (μ, λ) to (100, 0.05), (70, 0.1), (40, 0.15), respectively, and the average accuracy on seven context benchmarks is 90.47%, 90.75% and 90.53%.

Network Structure. Our architecture consists of the Glyph Pseudo-label Construction (GPC), Glyph Attention Network (GLAN) and Attention-based Character Fusion Module (ACFM). Our GLAN should be evaluated with GPC as a joint structure (JS) due to their interdependence (GLAN is supervised by glyph pseudo-labels from GPC). Thus we perform the “Baseline+JS” model to evaluate the effectiveness of our structure. As depicted in Table 6, the accuracy of “Baseline+JS” model is 6.53%, 5.13%, 0.65%, 0.88%, 1.15% higher than Baseline, SRN \dagger , PIMNet, ABINet \dagger , and S-GTR \dagger , respectively. Besides, we encapsulate the JS structure as a plug-in component to SRN \dagger and ABINet \dagger . As shown in the third group of rows in Table 6, after using our JS structure, the performance of these models is further improved by 5.45% and 1.11% on average accuracy, respec-

Table 6: Ablation study of the proposed SIGA structure on context benchmarks. “JS” means the joint structure of GPC and GLAN. They should be evaluated as a whole structure (GLAN needs GPC for glyph pseudo-label construction).

Methods	Datasets						Average 7248
	IIIT 3000	SVT 647	IC13 857	IC15 1811	SP 645	CT 288	
PIMNet	95.2	91.2	95.2	83.5	84.3	84.4	90.52
S-GTR \dagger	94.0	91.2	94.8	82.8	85.0	88.4	90.02
SRN \dagger	92.3	88.1	-	77.5	79.4	84.7	86.04
ABINet \dagger	94.7	91.7	95.0	82.7	85.1	86.5	90.29
Baseline	87.9	87.5	93.6	77.6	79.2	74.0	84.64
Baseline+JS	95.4	92.7	95.9	83.8	85.5	88.7	91.17
Baseline+JS+ACFM	95.7	93.8	96.2	84.3	86.2	90.0	91.67
ABINet \dagger +JS	95.3	91.5	96.5	84.6	85.3	91.7	91.40
SRN \dagger +JS	96.0	91.8	96.5	83.6	86.1	90.6	91.49

Table 7: Comparison results of speed and parameter amount.

Methods	Description	Size	Param. (MB)	Time (ms)
CA-FCN(VGG16)	Sup.	64 × 256	-	-
TextScanner(R50)	Sup.	64 × 256	57	56.8
SRN \dagger (R50+FPN)	Implicit	64 × 256	41.4	131.5
TRBA(R31)	Implicit	32 × 100	49.6	27.6
ABINet \dagger (R45)	Implicit	32 × 128	23.5	16.7
Ours(R45)	Self-Sup.	32 × 128	40.4	53.7

tively. These results demonstrate that the glyph attention extracted by the JS structure is effective and important to facilitate character recognition in the same two-dimensional space. Finally, the gain of adding ACFM is improved by 0.5%, from 91.17% to 91.67% on average accuracy.

Attention visualization. As shown in Figure 9, compared to a representative ABINet method, our method perceives more fine-grained structure information of glyphs. Especially, our attention can still degenerate into the same form of attention as other vision models in text images with very indistinct glyphs (e.g., the fifth group of rows in Figure 9).

Performance and Cost. We add speed and parameter comparisons in Table 7. For *supervised attention methods* with more parameters due to the large input size, e.g., 64 × 256, our method doesn’t need extra character-level annotations and has better performance than their methods in Table 2. For *implicit attention methods*, our method adds an unavoidable but acceptable amount of parameters (16.9M larger than ABINet \dagger , mainly used for a lightweight glyph attention structure) while obtaining more detailed glyph structures not being explored by other STR methods. Consequently, our method achieves the best performance on context and contextless benchmarks in Table 2 and 5.

Conclusions

In this paper, we propose a novel attention-based method for STR, Self-supervised Implicit Glyph Attention (SIGA). Beyond the difficulty of character-level annotation by humans, SIGA delineates the glyph structures of text images as the supervision of attention maps by jointly self-supervised text segmentation and implicit attention alignment. The learned glyph attention then encourages the text recognition network to focus on the structural regions of glyphs to improve attention correctness. Finally, extensive experiments demonstrate that SIGA achieves the best performance on context and contextless benchmarks.

References

- Arevalo, J.; Solorio, T.; Montes-y Gómez, M.; and González, F. A. 2017. Gated multimodal units for information fusion. *arXiv preprint arXiv:1702.01992*.
- Atienza, R. 2021. Vision Transformer for Fast and Efficient Scene Text Recognition. *arXiv preprint arXiv:2105.08582*.
- Baek, J.; Kim, G.; Lee, J.; Park, S.; Han, D.; Yun, S.; Oh, S. J.; and Lee, H. 2019. What is wrong with scene text recognition model comparisons? dataset and model analysis. In *Proceedings of the IEEE/CVF International Conference on Computer Vision (ICCV)*, 4715–4723.
- Baek, J.; Matsui, Y.; and Aizawa, K. 2021. What if we only use real datasets for scene text recognition? toward scene text recognition with fewer labels. In *Proceedings of the IEEE/CVF Conference on Computer Vision and Pattern Recognition (CVPR)*, 3113–3122.
- Bai, F.; Cheng, Z.; Niu, Y.; Pu, S.; and Zhou, S. 2018. Edit probability for scene text recognition. In *Proceedings of the IEEE/CVF Conference on Computer Vision and Pattern Recognition (CVPR)*, 1508–1516.
- Bhunia; and et al. 2021. Joint visual semantic reasoning: Multi-stage decoder for text recognition. In *Proceedings of the IEEE/CVF International Conference on Computer Vision (ICCV)*, 14940–14949.
- Bhunia, A. K.; Ghose, S.; Kumar, A.; Chowdhury, P. N.; Sain, A.; and Song, Y.-Z. 2021. Metaht: Towards writer-adaptive handwritten text recognition. In *Proceedings of the IEEE/CVF conference on computer vision and pattern recognition (CVPR)*, 15830–15839.
- Biten, A. F.; Tito, R.; Mafla, A.; Gomez, L.; Rusinol, M.; Valveny, E.; Jawahar, C.; and Karatzas, D. 2019. Scene text visual question answering. In *Proceedings of the IEEE/CVF international conference on computer vision*, 4291–4301.
- Cheng, Z.; Bai, F.; Xu, Y.; Zheng, G.; Pu, S.; and Zhou, S. 2017. Focusing attention: Towards accurate text recognition in natural images. In *Proceedings of the IEEE/CVF International Conference on Computer Vision (ICCV)*, 5076–5084.
- Fang, S.; Xie, H.; Wang, Y.; Mao, Z.; and Zhang, Y. 2021. Read Like Humans: Autonomous, Bidirectional and Iterative Language Modeling for Scene Text Recognition. In *Proceedings of the IEEE/CVF Conference on Computer Vision and Pattern Recognition (CVPR)*, 7098–7107.
- Guan, T.; Gu, C.; Lu, C.; Tu, J.; Feng, Q.; Wu, K.; and Guan, X. 2022. Industrial Scene Text Detection with Refined Feature-attentive Network. *IEEE Transactions on Circuits and Systems for Video Technology (TCSVT)*.
- Gupta, A.; Vedaldi, A.; and Zisserman, A. 2016. Synthetic data for text localisation in natural images. In *Proceedings of the IEEE/CVF Conference on Computer Vision and Pattern Recognition (CVPR)*, 2315–2324.
- Hartigan, J. A.; and Wong, M. A. 1979. Algorithm AS 136: A k-means clustering algorithm. *Journal of the royal statistical society. series c (applied statistics)*, 28(1): 100–108.
- He, K.; Zhang, X.; Ren, S.; and Sun, J. 2016. Deep residual learning for image recognition. In *Proceedings of the IEEE/CVF Conference on Computer Vision and Pattern Recognition (CVPR)*, 770–778.
- He, Y.; Chen, C.; Zhang, J.; Liu, J.; He, F.; Wang, C.; and Du, B. 2022. Visual semantics allow for textual reasoning better in scene text recognition. In *Proceedings of the AAAI Conference on Artificial Intelligence (AAAI)*, volume 36, 888–896.
- Jaderberg, M.; Simonyan, K.; Vedaldi, A.; and Zisserman, A. 2014. Synthetic data and artificial neural networks for natural scene text recognition. *arXiv preprint arXiv:1406.2227*.
- Jaderberg, M.; Simonyan, K.; Zisserman, A.; et al. 2015. Spatial transformer networks. *Advances in Neural Information Processing Systems (NIPS)*, 28: 2017–2025.
- Kenton, J. D. M.-W. C.; and Toutanova, L. K. 2019. BERT: Pre-training of Deep Bidirectional Transformers for Language Understanding. In *Proceedings of NAACL-HLT*, 4171–4186.
- Kingma, D. P.; and Ba, J. 2014. Adam: A method for stochastic optimization. *arXiv preprint arXiv:1412.6980*.
- Lee, J.; Park, S.; Baek, J.; Oh, S. J.; Kim, S.; and Lee, H. 2020. On recognizing texts of arbitrary shapes with 2D self-attention. In *Proceedings of the IEEE/CVF Conference on Computer Vision and Pattern Recognition Workshops*, 546–547.
- Li, H.; Wang, P.; Shen, C.; and Zhang, G. 2019. Show, attend and read: A simple and strong baseline for irregular text recognition. In *Proceedings of the AAAI Conference on Artificial Intelligence (AAAI)*, 8610–8617.
- Liao, M.; Zhang, J.; Wan, Z.; Xie, F.; Liang, J.; Lyu, P.; Yao, C.; and Bai, X. 2019. Scene text recognition from two-dimensional perspective. In *Proceedings of the AAAI Conference on Artificial Intelligence (AAAI)*, 8714–8721.
- Liu, Z.; Li, Y.; Ren, F.; Goh, W. L.; and Yu, H. 2018. Squeezedtext: A real-time scene text recognition by binary convolutional encoder-decoder network. In *Proceedings of the AAAI Conference on Artificial Intelligence (AAAI)*, volume 32.
- Luo, C.; Jin, L.; and Sun, Z. 2019. Moran: A multi-object rectified attention network for scene text recognition. *Pattern Recognition (PR)*, 90: 109–118.
- Lyu, P.; Liao, M.; Yao, C.; Wu, W.; and Bai, X. 2018. Mask textspotter: An end-to-end trainable neural network for spotting text with arbitrary shapes. In *Proceedings of the European Conference on Computer Vision (ECCV)*, 67–83.
- Milletari, F.; Navab, N.; and Ahmadi, S.-A. 2016. V-net: Fully convolutional neural networks for volumetric medical image segmentation. In *2016 fourth international conference on 3D vision (3DV)*, 565–571. IEEE.
- Mou, Y.; Tan, L.; Yang, H.; Chen, J.; Liu, L.; Yan, R.; and Huang, Y. 2020. Plugnet: Degradation aware scene text recognition supervised by a pluggable super-resolution unit. In *Proceedings of the European Conference on Computer Vision (ECCV)*, 158–174. Springer.
- Neumann, L.; and Matas, J. 2012. Real-time scene text localization and recognition. In *Proceedings of the IEEE/CVF Conference on Computer Vision and Pattern Recognition (CVPR)*, 3538–3545. IEEE.

- Qiao, Z.; Zhou, Y.; Wei, J.; Wang, W.; Zhang, Y.; Jiang, N.; Wang, H.; and Wang, W. 2021. PIMNet: a parallel, iterative and mimicking network for scene text recognition. In *Proceedings of the 29th ACM International Conference on Multimedia (ACM MM)*, 2046–2055.
- Qiao, Z.; Zhou, Y.; Yang, D.; Zhou, Y.; and Wang, W. 2020. SEED: Semantics Enhanced Encoder-Decoder Framework for Scene Text Recognition. In *arXiv*.
- Shi, B.; Bai, X.; and Yao, C. 2016. An end-to-end trainable neural network for image-based sequence recognition and its application to scene text recognition. *IEEE Transactions on Pattern Analysis and Machine Intelligence (TPAMI)*, 39(11): 2298–2304.
- Shi, B.; Wang, X.; Lyu, P.; Yao, C.; and Bai, X. 2016. Robust scene text recognition with automatic rectification. In *Proceedings of the IEEE/CVF Conference on Computer Vision and Pattern Recognition (CVPR)*, 4168–4176.
- Shi, B.; Yang, M.; Wang, X.; Lyu, P.; Yao, C.; and Bai, X. 2018. Aster: An attentional scene text recognizer with flexible rectification. *IEEE Transactions on Pattern Analysis and Machine Intelligence (TPAMI)*, 41(9): 2035–2048.
- Smith, L. N.; and Topin, N. 2019. Super-convergence: Very fast training of neural networks using large learning rates. In *Artificial intelligence and machine learning for multi-domain operations applications*, volume 11006, 1100612. International Society for Optics and Photonics.
- Wan, Z.; He, M.; Chen, H.; Bai, X.; and Yao, C. 2020. Textscanner: Reading characters in order for robust scene text recognition. In *Proceedings of the AAAI Conference on Artificial Intelligence (AAAI)*, 12120–12127.
- Wang, D.-H.; Liu, C.-L.; Yu, J.-L.; and Zhou, X.-D. 2009. CASIA-OLHWDB1: A database of online handwritten Chinese characters. In *International Conference on Document Analysis and Recognition (ICDAR)*, 1206–1210. IEEE.
- Wang, K.; and Belongie, S. 2010. Word spotting in the wild. In *Proceedings of the European Conference on Computer Vision (ECCV)*, 591–604. Springer.
- Wang, T.; Zhu, Y.; Jin, L.; Luo, C.; Chen, X.; Wu, Y.; Wang, Q.; and Cai, M. 2020. Decoupled attention network for text recognition. In *Proceedings of the AAAI Conference on Artificial Intelligence (AAAI)*, 12216–12224.
- Wang, Y.; Xie, H.; Fang, S.; Wang, J.; Zhu, S.; and Zhang, Y. 2021. From two to one: A new scene text recognizer with visual language modeling network. In *Proceedings of the IEEE/CVF International Conference on Computer Vision (ICCV)*, 14194–14203.
- Yang, M.; Guan, Y.; Liao, M.; He, X.; Bian, K.; Bai, S.; Yao, C.; and Bai, X. 2019. Symmetry-constrained rectification network for scene text recognition. In *Proceedings of the IEEE/CVF International Conference on Computer Vision (ICCV)*, 9147–9156.
- Yu, D.; Li, X.; Zhang, C.; Liu, T.; Han, J.; Liu, J.; and Ding, E. 2020. Towards accurate scene text recognition with semantic reasoning networks. In *Proceedings of the IEEE/CVF Conference on Computer Vision and Pattern Recognition (CVPR)*, 12113–12122.
- Zhang, C.; Xu, Y.; Cheng, Z.; Pu, S.; Niu, Y.; Wu, F.; and Zou, F. 2021. SPIN: Structure-preserving inner offset network for scene text recognition. In *Proceedings of the AAAI Conference on Artificial Intelligence (AAAI)*, volume 35, 3305–3314.